Supplement of The Cryosphere, 19, 6807–6826, 2025
https://doi.org/10.5194/tc-19-6807-2025-supplement

The Cryosphere
Open Access

Supplement of

Quantifying the interplay of sea ice meltwater and ice–albedo feedbacks in the Arctic ice-ocean system

Haohao Zhang et al.

Correspondence to: Xuezhi Bai (xuezhi.bai@hhu.edu.cn)

S1 One-Dimensional Coupled Sea Ice-Ocean Model Equations

S1.1 Ocean Module

The ocean module governs the evolution of potential temperature T and salinity S in the water column:

$$\frac{\partial T}{\partial t} = \frac{\partial}{\partial z}\left(K_T \frac{\partial T}{\partial z}\right) + \gamma_T + \frac{Q_{sw}}{\rho c_p} \tag{S1}$$

$$\frac{\partial S}{\partial t} = \frac{\partial}{\partial z}\left(K_S \frac{\partial S}{\partial z}\right) + \gamma_S \tag{S2}$$

where, ρ is seawater density (kg/m^3); c_p is specific heat capacity of seawater (J/ (kg °C)); $K_T = K_{bg} + K_{kpp,T}$ and $K_S = K_{bg} + K_{kpp,S}$ (m^2/s) are the total vertical diffusion coefficient for temperature and salinity, respectively. Q_{sw} (W/m^2) is the heat source from absorbed shortwave radiation. K_{bg} is the background vertical diffusivity. $K_{kpp,T}$ and $K_{kpp,S}$ are the turbulent mixing within the boundary layer calculated by the KPP scheme (Large et al., 1994).

$$K_T = K_{bg} + K_{kpp,T} \tag{S3}$$

$$K_S = K_{bg} + K_{kpp,S} \tag{S4}$$

$$K_{kpp,x}(\sigma) = h \cdot w_x(\sigma) \cdot G(\sigma) \quad (x = T, S) \tag{S5}$$

where, $\sigma = d/h$ $(d \leq h)$ is the non-dimensional depth; $d = -z$ is the distance from the sea surface; h is the boundary layer depth; $w_x(\sigma)$ is the turbulent velocity scale; $G(\sigma)$ is the shape function, with coefficients determined by matching surface similarity theory and interior diffusivity at the base of the boundary layer (see Large et al. 1994 for more details). γ_T (°C/s) and γ_S (psu/s) are non-local transport terms for temperature and salinity, respectively. The non-local transport term is activated only under unstable convective conditions:

$$\gamma_x = C_x \frac{w_x^0}{w_x(\sigma)h} \tag{S6}$$

where, w_x^0 is the Surface kinematic flux; C_x is a constant. The boundary layer depth h is determined by the depth where the bulk Richardson number, and the boundary layer depth h is equated to the smallest value of d at which this Richardsonnumber equals a critical value Ri_c $(= 0.3)$. The bulk Richardson number is:

$$Ri_b(d) = \frac{\left(B_r - B(d)\right) \cdot d}{|V_r - V(d)|^2 + V_t^2(d)} \tag{S7}$$

where, $B = g(\alpha T - \beta S)$ (m/s^2) is the Seawater buoyancy; g (m/s^2) is the Gravitational acceleration; α and β are the Thermal expansion coefficient and haline contraction coefficient, respectively; B_r and V_r are the Buoyancy and horizontal velocity in the near-surface reference layer, respectively; $B(d)$ and $V(d)$ are the Buoyancy and velocity at depth d, respectively; $V_t(d)$ is the Turbulent velocity shear term at depth d.

The ocean surface (at $z = 0\ m$) boundary conditions are:

$$K_\theta \frac{\partial\theta}{\partial z} = \frac{Q_{net}}{\rho c_p}, \quad K_S \frac{\partial S}{\partial z} = \frac{F_S}{\rho} \tag{S8}$$

where Q_{net} (W/m^2) is net heat flux into the ocean; F_S (psu·m/s) is surface salinity flux caused by the ice melting/freezing and other freshwater flux.

The ocean bottom (at $z = 700\ m$) is closed boundary with no flux:

$$\frac{\partial\theta}{\partial z} = 0, \quad \frac{\partial S}{\partial z} = 0 \tag{S9}$$

S1.2 Sea Ice Module

The sea ice module is a two-layer thermodynamic model based on Winton, (2000) and the LANL CICE model (Bitz and Lipscomb, 1999). It considers two equally thick ice layers with the upper layer having variable specific heat due to brine pockets, and the lower layer is treated as pure ice with fixed heat capacity. A snow layer with zero heat capacity lies above the ice. The sea ice module can calculate the energy flux at the surface available for melting (if $T_s = 0$) and the energy at the ocean-ice interface for either melting or freezing.

$$E_{top} = \left(Q_{net,ice} - K_{1/2}(T_s - T_1)\right)\Delta t \tag{S10}$$

$$E_{bot} = (F_{cb} - F_{oi})\Delta t \tag{S11}$$

where, $Q_{net,ice}$ is the heat flux at the ice/snow surface; $K_{1/2} = \frac{4K_iK_s}{K_sh_i+4K_ih_s}$, K_i and K_s are constant thermal conductivities of sea ice and snow; T_s is the skin temperature; T_1 and T_2 are the two layers of ice temperatures; T_f is the sea surface temperature which set to freezing point; F_{cb} is the heat flux conducted through ice to bottom surface; F_{oi} is the heat flux at the ice bottom due to the sea surface temperature variations from freezing point:

$$F_{cb} = \frac{4K_i(T_2 - T_f)}{h_i} \tag{S12}$$

$$F_{oi} = c_{sw}\rho_{sw}\gamma\left(T_{SST} - T_f\right)u^*, \ (T_{SST} > T_f) \tag{S13}$$

$$F_{oi} = \left(T_f - T_{SST}\right)c_f\rho_f\frac{\Delta z}{\Delta t}\ , \ (T_{SST} < T_f) \tag{S14}$$

where, c_{sw} and ρ_{sw} are the heat capacity and density of the seawater, respectively. γ (= 0.006) is the heat transfer coefficient. c_f $(= 4180\ J/(kg\ °C))$ and ρ_f $(= 1000\ kg/m^3)$ are the specific heat capacity and density of liquid freshwater, respectively. The friction velocity $u^* = \sqrt{|\tau_w|/\rho_{sw}}$ is the frictional velocity between ice and water, with minimum value of $u^*(= 0.005)$, where τ_w is the ice-ocean stress.

If $E_{top} > 0$ the module melts snow from the surface, if all the snow is melted and there is energy left, the module melts the ice. If the ice is all gone and there is still energy left, the module applies the left-over energy to heating the ocean model upper layer (Winton, 2000). Similarly, if $E_{bot} > 0$, the module melts ice from the bottom. If all the ice is melted, the snow is melted (with energy from the ocean model upper layer if necessary). If $E_{bot} < 0$ we grow ice at the bottom

$$\Delta h_i = \frac{-E_{bot}}{q_{bot}\rho_i} \tag{S15}$$

where q_{bot} is the enthalpy of the new ice; ρ_i $(= 900\ kg/m^3)$ is the ice density. If there is an ice layer and the overlying air temperature is below $0°C$ then any precipitation, P joins the snow layer:

$$\Delta h_s = -P\frac{\rho_f}{\rho_s}\Delta t \tag{S16}$$

where, ρ_s $(= 330\ kg/m^3)$ is the fresh water and snow densities.

S1.3 Albedo Parameterization

The ice albedo varies with ice thickness:

$$\alpha_{ice} = \alpha_{ice,max} + (\alpha_{ice,min} - \alpha_{ice,max})exp\left(-\frac{h_i}{h_{albice}}\right) \tag{S17}$$

where, $\alpha_{ice,min}(= 0.2)$ and $\alpha_{ice,max}(= 0.66)$ are ice albedos for thin and thick bare ice respectively. h_i is the ice thickness and h_{albice} $(= 0.8)$ is the scale of ice albedo decay.

Snow albedo depends on surface temperature and snow age:

$$\alpha_{snow} = \alpha_{oldsnow} + (\alpha_{newsnow} - \alpha_{oldsnow})exp\left(-0.2 \cdot S_{days}\right) \tag{S18}$$

where, $\alpha_{oldsnow}(= 0.55)$ is the old snow albedo. S_{days} is the Snow age. $\alpha_{new\ snow}$ is the Fresh snow albedo:

$$\alpha_{newsnow} = \alpha_{coldsnow} + (\alpha_{warmsnow} - \alpha_{coldsnow})max\left(0, min\left(1 - \frac{T_s}{T_{snow,alb}}, 1\right)\right) \quad \text{(S19)}$$

where, $\alpha_{coldSnow}$ $(= 0.85)$ and $\alpha_{warmSnow}$ $(= 0.7)$ are snow albedos for cold and warm snow respectively. $T_{snow,alb}$ $(= 10°\text{C})$ is a temperature threshold parameter.

Snow and ice albedo are combined with snow thickness attenuation:

$$\alpha = \alpha_{snow} + (\alpha_{ice} - \alpha_{snow})exp\left(-\frac{h_s}{h_{albsnow}}\right) \quad \text{(S20)}$$

where, $h_{albsnow}$ $(= 0.3)$ is a scale height for snow albedo. h_s is the snow thickness.

S1.4 Shortwave Radiation Penetration Parameterization

Shortwave radiation entering the ocean is partitioned based on surface state (open ocean or ice-covered). The net shortwave flux entering the ocean $Q_{sw,ocn}$ is a weighted average based on sea ice concentration A_{ice} $(0 - 1)$:

$$Q_{sw,ocn} = (1 - A_{ice})Q_{sw,ocn,open} + A_{ice}Q_{sw,ocn,ice} \quad \text{(S21)}$$

where, $Q_{sw,ocn,open}$ is the shortwave radiation entering the ocean from open-ocean; $Q_{sw,ocn,ice}$ is the shortwave radiation entering the ocean from ice-covered area:

$$Q_{sw,ocn,open} = (1 - \alpha_{oce})F_{SW} \quad \text{(S22)}$$

$$Q_{sw,ocn,ice} = Q_{sw,pen} \cdot exp(-k_{solar}h_{ice}) \quad \text{(S23)}$$

where, α_{oce} $(= 0.08)$ is the sea surface albedo; F_{SW} is the downward shortwave radiation forcing; k_{solar} $(= 1.5\, m^{-1})$ is the sea ice volume extinction coefficient; h_{ice} is the sea ice thickness (m); $Q_{sw,pen}$ is the radiation penetrating the ice surface:

$$Q_{sw,pen} = (1 - \alpha_{is})F_{SW} \cdot (1 - f_s)i0swFrac \quad \text{(S24)}$$

where, f_s $(0 - 1)$ is the fractional snow cover; $i0swFrac$ $(= 0.3)$ is the fraction of radiation penetrating the ice surface (dimensionless parameter); α_{is} is the ice/snow albedo.

Shortwave radiation decays exponentially with depth z using a two-band model (Paulson and Simpson, 1977):

$$Q_{sw}(z) = Q_{sw,ocn}\left[r exp\left(-\frac{z}{\lambda_1}\right) + (1-r) exp\left(-\frac{z}{\lambda_2}\right)\right] \tag{S25}$$

where, $Q_{sw}(z)$ is the shortwave radiation at depth z; r is the fraction of radiation in the first (rapidly attenuating) band; $\lambda_1 (= 0.6\ m)$ and $\lambda_2 (= 20\ m)$ are the attenuation length scale for the first and second band. Below 200 m depth, the penetration fraction is set to zero.

S2 Model Validation

S2.1 Validation of Background mixing coefficient

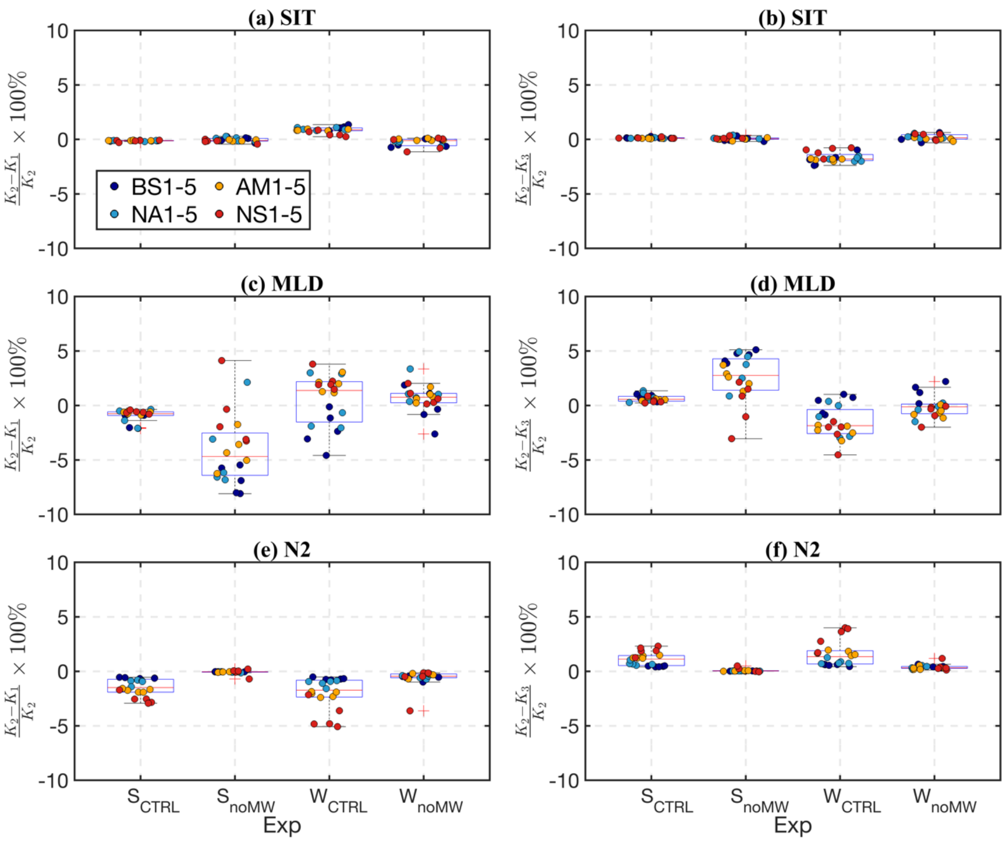

Figure S1. Percent differences in (a)–(b) sea ice thickness and (c)–(d) mixed layer depth and (e)-(f) upper 500 m buoyancy frequency between summer and winter averages derived using different background mixing coefficients ($K_1 = 10^{-7}\ m^2 s^{-1}$; $K_2 = 5.44 \times 10^{-7}\ m^2 s^{-1}$; $K_3 = 10^{-6}\ m^2 s^{-1}$). On the horizontal axis, Sctrl and SnoMW denote results from the summer control and no-meltwater experiments, respectively, while Wctrl and WnoMW represent those from the winter control and no-meltwater experiments. All points are the results of experiments with initial SIT of 1.5 m.

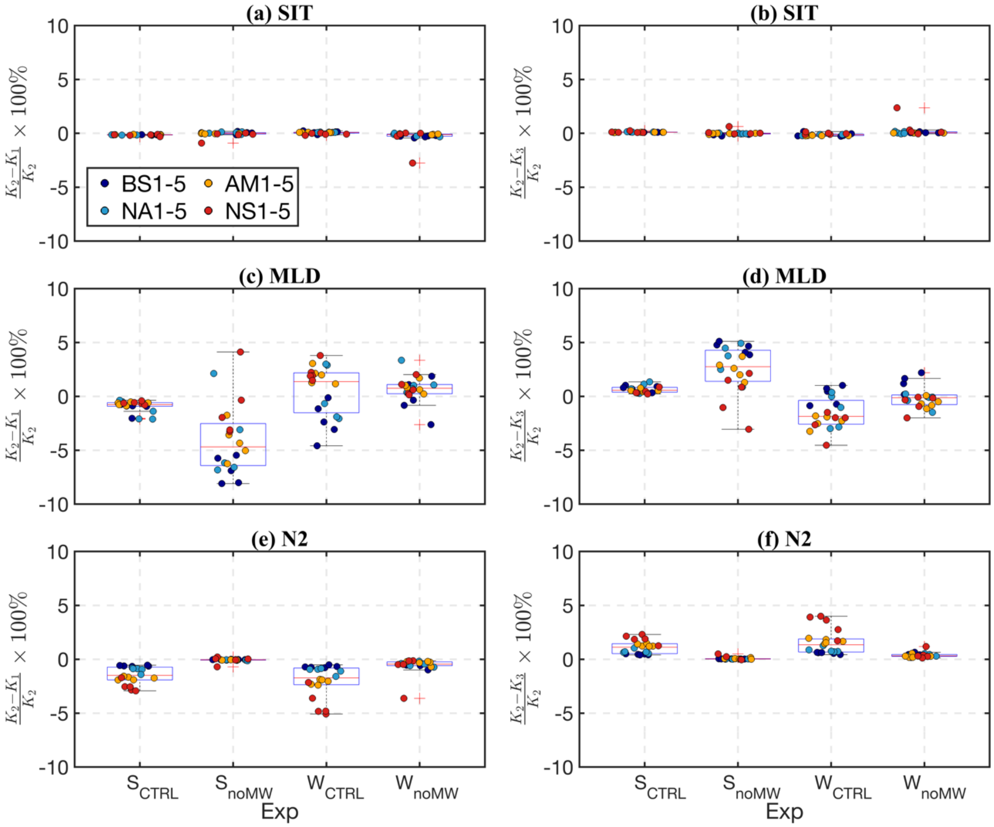

Figure S2. Same as Figure S1, but for the results of experiments with initial SIT of 2 m.

S2.2 Validation of boundary conditions at the bottom

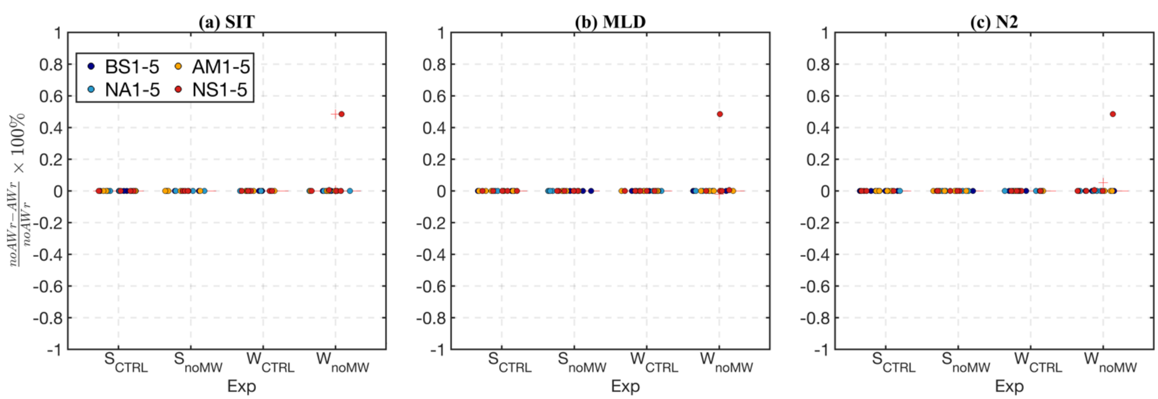

Figure S3. Percent differences in (a) sea ice thickness and (b) mixed layer depth and (c) upper 500 m buoyancy frequency between summer and winter averages derived using different bottom boundary conditions (noAWr: closed boundary condition; AWr: one-day recovery boundary condition). On the horizontal axis, S_{ctrl} and S_{noMW} denote results from the summer control and no-meltwater

experiments, respectively, while W_{CTRL} and W_{noMW} represent those from the winter control and no-meltwater experiments. All points are the results of experiments with initial SIT of 1.5 m.

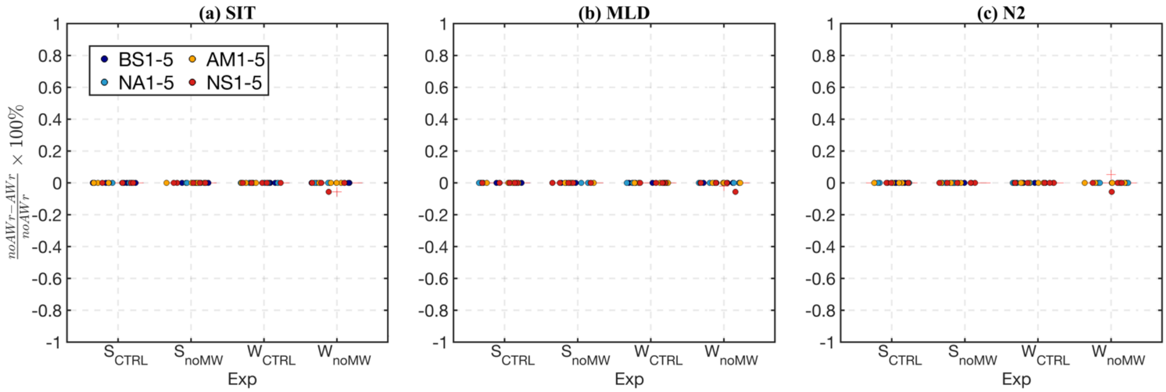

Figure S4. Same as Figure S3, but for the results of experiments with initial SIT of 2 m.

S2.3 External freshwater forcing

In order to verify the external freshwater forcing values of 1200 km³/yr is reasonable, we conducted experiments using external freshwater forcing values of 6400 km³/yr (Runoff plus P-E, as described by Haine et al., 2015), 1200 km³/yr (sum of Runoff, P-E, and the net flow through arctic straits), as well as zero external freshwater forcing. The results show that a forcing value of 6400 km^3 causes excessive freshwater accumulation at the surface, resulting in a maximum mixed layer depth (MLD) of only ~ 25 m in winter across all regions (Figure. S5, blue lines). This is clearly unreasonable compared to observed values, which shows the MLD in the Canadian Basin is approximately 30 m, and in the Eurasian Basin, it ranges from about 70 to over 100 m during winter (Peralta-Ferriz and Woodgate, 2015). In contrast, the experimental results using a freshwater forcing of 1200 km³/yr are much more reasonable and closer to the observations. (Figure. S5, black lines). The experimental results using zero freshwater forcing are also close to the observations but deeper than 1200 km³/y (Figure. S5, red lines) but also agree with the observations. We also examined the meltwater feedback values under different external freshwater forcing scenarios. The results show that neglecting external freshwater forcing slightly exaggerates the strength of the meltwater feedback compared to including a forcing of 1200 km³/yr, with the feedback value increasing in magnitude from -0.19 to -0.2 (Figure. S6). In contrast, when a forcing of

6400 km³/yr is considered, the meltwater feedback decreases to -0.05; however, it has been demonstrated that 6400 km³/yr is an unrealistic value (Figure. S6).

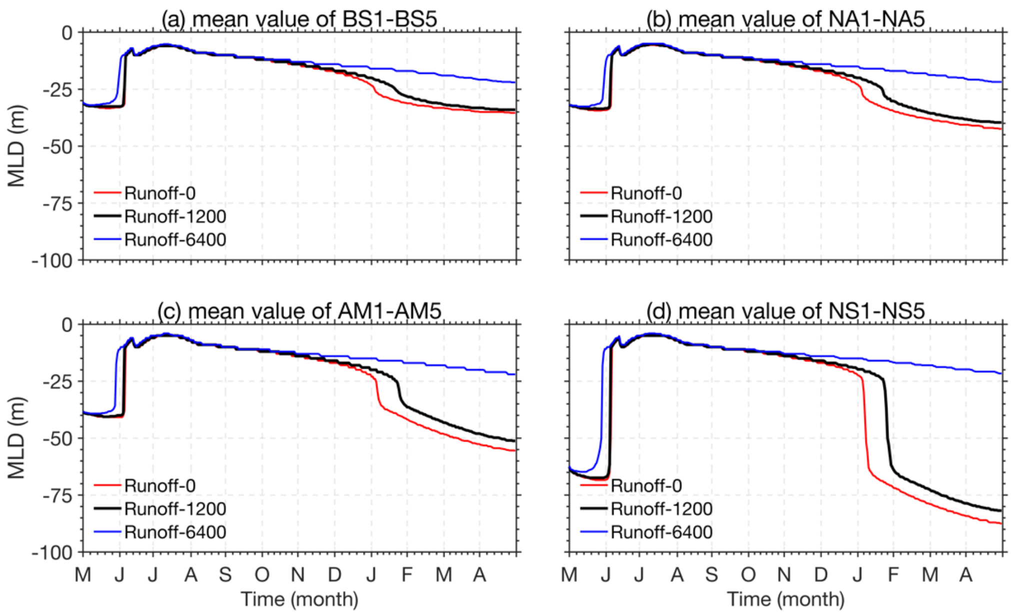

Figure S5. Time series of the mean MLD for each basin, obtained from simulations using external freshwater forcing values of 0 km³/y, 1200 km³/y and 6400 km³/y.

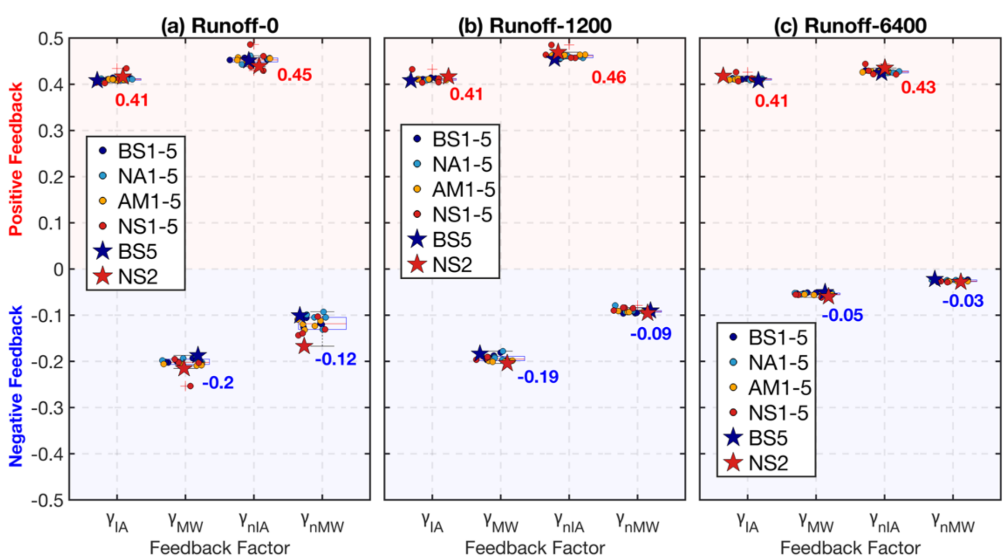

Figure S6. Box plots illustrate the four feedback factors across different stations, with external freshwater forcing values of (a) 0 km³/y, (b) 1200 km³/y and (c) 6400 km³/y.

S2.4 Comparison with observations

In the CTRL run, the simulated average minimum summer sea ice thickness across all 20 stations is 0.91 ± 0.04 m, which closely matching the observed value of 0.82 ± 0.11 m in the Arctic Ocean at the end of the melting season during 2011-2020 (Landy et al., 2022). This indicates that the sea ice results from our 1D model align well with actual Arctic sea ice conditions. The summer ice melt is approximately 1.1 m (as shown in Figure 4a in the main text), which is equivalent to 1 m of freshwater released to the ocean. This is close to the value of about 1.2 m sea ice meltwater reported by Haine et al., (2015). While our estimate is slightly lower, it is reasonable considering that melt rates in the coastal marginal ice zone are generally higher than those in the central deep basin. As for albedo values, recent studies based on MOSAiC data indicate that the observed albedo ranges from approximately 0.55 to 0.64 across thin ice (less than 0.5 m) to thick ice (greater than 1 m), with relatively stable values for ice thicker than 1 m (Light et al., 2022). In our simulations, summer sea ice thins from 2.0 m to 0.9 m, accompanied by a decrease in albedo from 0.63 to 0.58. These results suggest that our simulated albedo values are in the range of observations.

The 1D model used in this study also reproduces the seasonal changes in the vertical structure of the Arctic Ocean well. Statistical analysis of various hydrographic profile observations shows that the MLDs during July and August are 8.7 ± 3.6 m in the Canadian Basin and 22 ± 13 m in the Eurasian Basin (Peralta-Ferriz and Woodgate, 2015). The model results show similar summer mixed layer depth (MLD) values across stations under the same threshold criterion and month time, with an average summer MLD of ~7.6 m in the CTRL runs, which means the simulated values in the Canadian Basin closely match the observations, while those in the Eurasian Basin are relatively shallow.

In the Eurasian Basin, the inflow of highly saline Atlantic water drives interactions between the seasonal mixed layer and the ocean interior (Polyakov et al., 2017). Because this 1D model simulations exclude advection flux processes and the Eurasian Basin is more saline, the surface layer is more susceptible to a larger salinity gradient due to the lack of advection-replenished saline water and the continuous release of freshwater from ice melting, which may contribute to the modelled shallower summer MLD. In winter, the observed April MLDs are approximately 33 ± 8 m in the Canadian Basin and ~70 to 100+ m in the Eurasian Basin. Our simulations show that the average MLD in April is ~35 m for all CTRL runs in the Canadian Basin and ~70 m in the Eurasian Basin. In particular, the MLD can exceed 100 m in April at stations NS2 and NS4. Our model also accurately reproduces the appearance and changes of the NSTM (such as Figure. 5a in the main text), which is the remnant solar heat trapped beneath the ML and a notable feature in the Canadian Basin, caused by penetrative shortwave solar heating principally through leads (Jackson et al., 2010; Maykut and McPhee, 1995; Steele et al., 2011).

In addition, the ITP41 captured NSTM changes very well and had short spatial drift between May 2011 and April 2012. We further validated the model by simulating the ITP41 case with its corresponding atmospheric forcing field and initial conditions, and the results show the model's capability to replicate the observed seasonal thermohaline variations (Figure. S7). Based on the observations, the ocean-to-ice heat flux (F_{oi}) has a significant seasonal cycle with maximum values reaching 40-60 W/m^2 in summer (Maykut and McPhee, 1995) and close to zero during winter in many instances (Krishfield and Perovich, 2005; McPhee et al., 2003; Zhong et al., 2022). The model results of the CTRL agree with the observed values well (Figure 8a and b in main text).

In conclusion, our 1D model simulated summer ice condition and seasonal variations in the vertical structure of the Arctic Ocean in qualitative agreement with observations. While the CTRL run does not aim to precisely replicate observed values, it provides a baseline of reasonable accuracy for comparing differences between CTRL and sensitivity experiments.

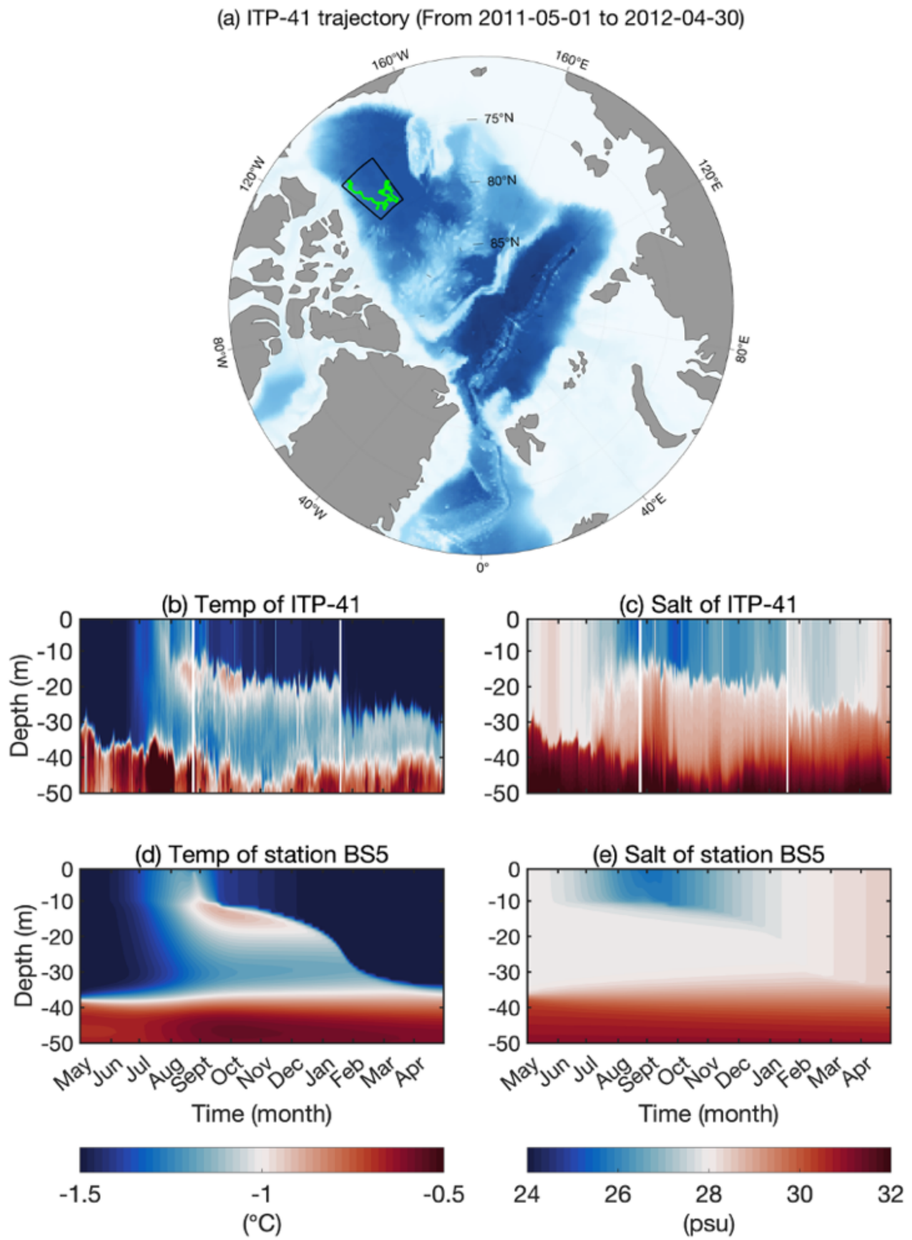

Figure S7. (a) Trajectory of ITP 41 from May 2011 to April 2012 shown in green. In this case simulation, the atmospheric forcing field is derived from NCEP-DOE (https://psl.noaa.gov) and averaged over the region outlined by the black line, covering the same time as ITP 41. Initial ice and snow thicknesses are taken from NSIDC (https://nsidc.org/data/nsidc-0773/versions/1) regional averages for May 2011. (b)–(e): Time series of temperature (left column) and salinity (right column) in the upper 50 m, derived from (b, c) ITP 41 observations and (d, e) simulation results.

S3 Model results for experiments with initial SIT of 1.5 m

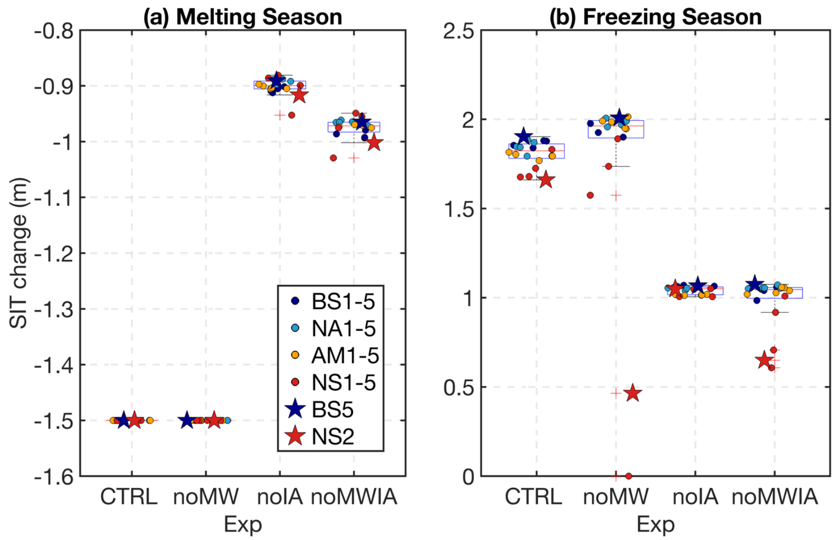

Figure S8. Box plots illustrating the (a) ice thickness changes during the melting season and (b) freezing season across different Stations in different types of experiments. Each box plot shows the median, interquartile range, and potential outliers (points marked with red plus sign). All points are the results of experiments with initial SIT of 1.5 m. The blue star and red star represent stations BS5 and NS2, respectively.

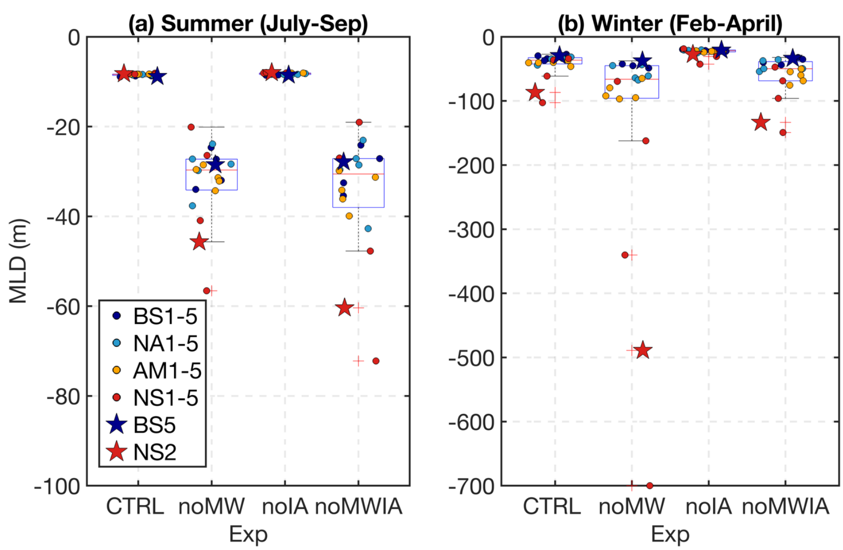

Figure S9. Box plots illustrating the mean (a) MLD in summer and (b) winter across different Stations in different types of experiments. Each box plot shows the median, interquartile range, and potential outliers (points marked with red plus sign). All points are the results of experiments with initial SIT of 1.5 m. The blue star and red star represent stations BS5 and NS2, respectively.

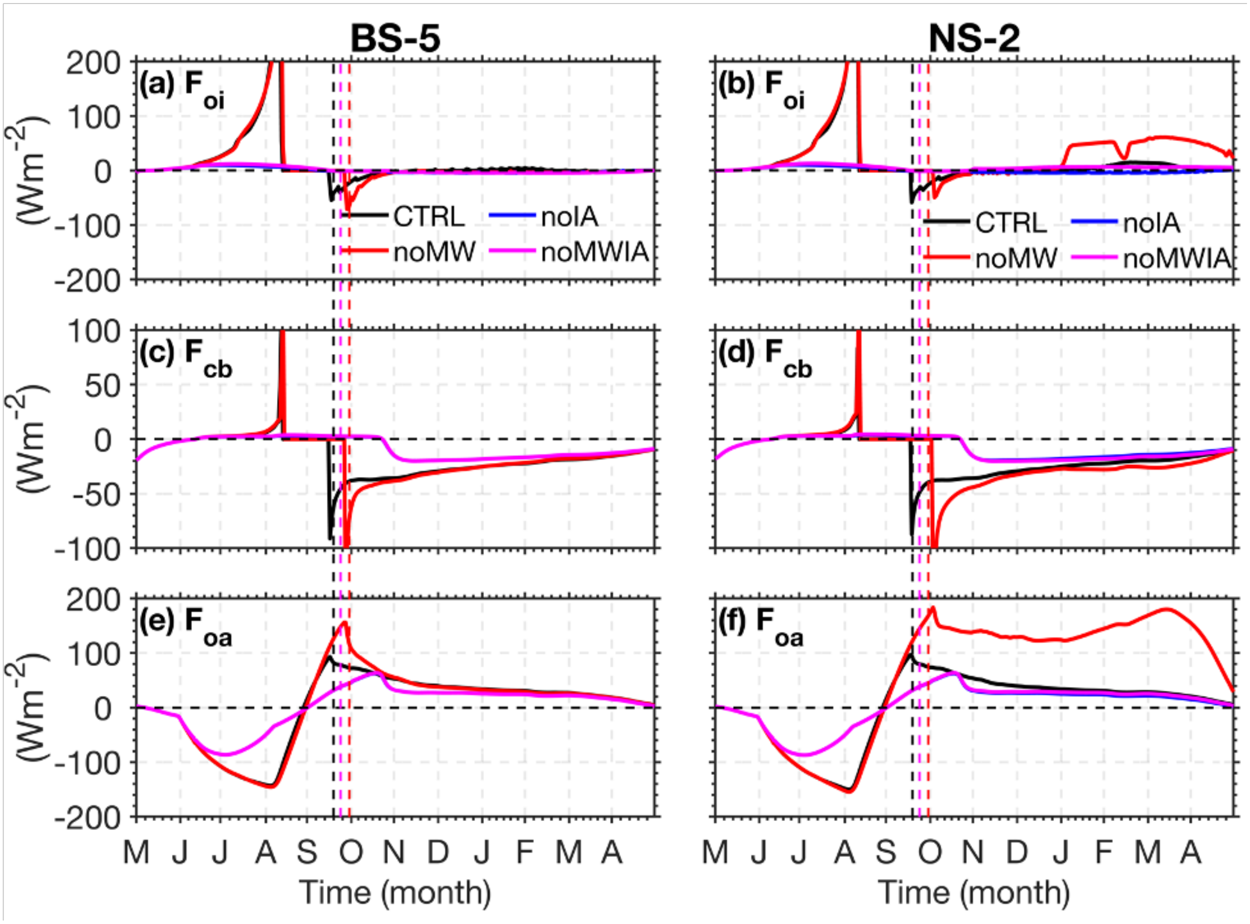

Figure S10. Heat flux time series at station BS5 (left column) and NS2 (right column). (a)-(b): F_{oi} (ocean-to-ice heat flux); (c)-(d): F_{cb} (heat flux conduct through ice to bottom surface); (e)-(f): F_{oa} (ocean-atmosphere heat flux over the open ocean) for the experiments with initial SIT of 1.5 m. In the panels of (a)-(d), positive (negative) values denote heat gain (loss) at the ice base. In the panels of (e)-(f), positive (negative) values denote upward (downward) heat flux, corresponding to oceanic heat loss (gain).

S4 Model results using climatological initial conditions

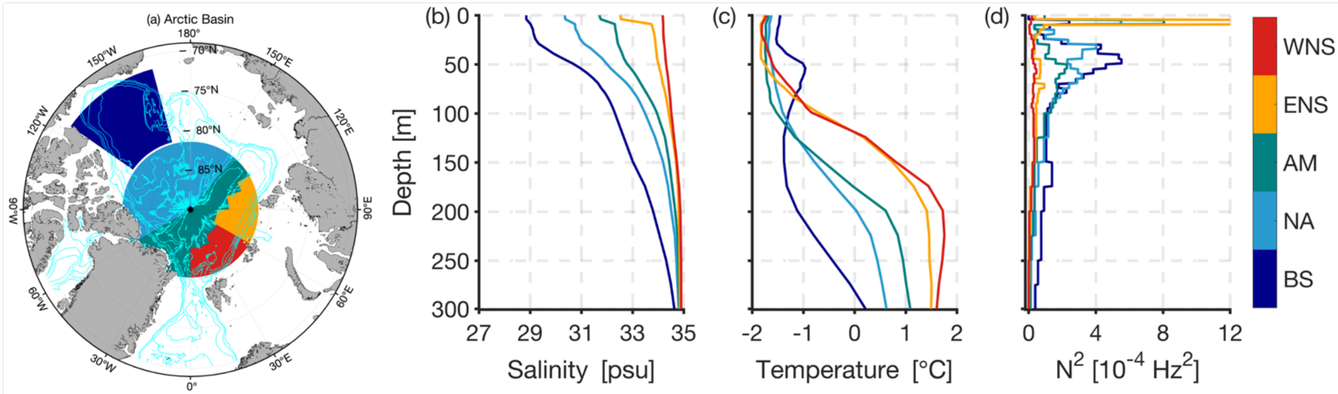

Figure S11. (a) Five sub-regions in the Arctic Ocean simulated using WOA2023 climatological data as the initial condition. BS: Beaufort Sea; NA: North of the Amerasian Basin; AM: Amundsen Basin; ENS: Eastern Nansen Basin; WNS: Western Nansen Basin. Corresponding profiles show (b) salinity, (c) temperature, and (d) buoyancy frequency.

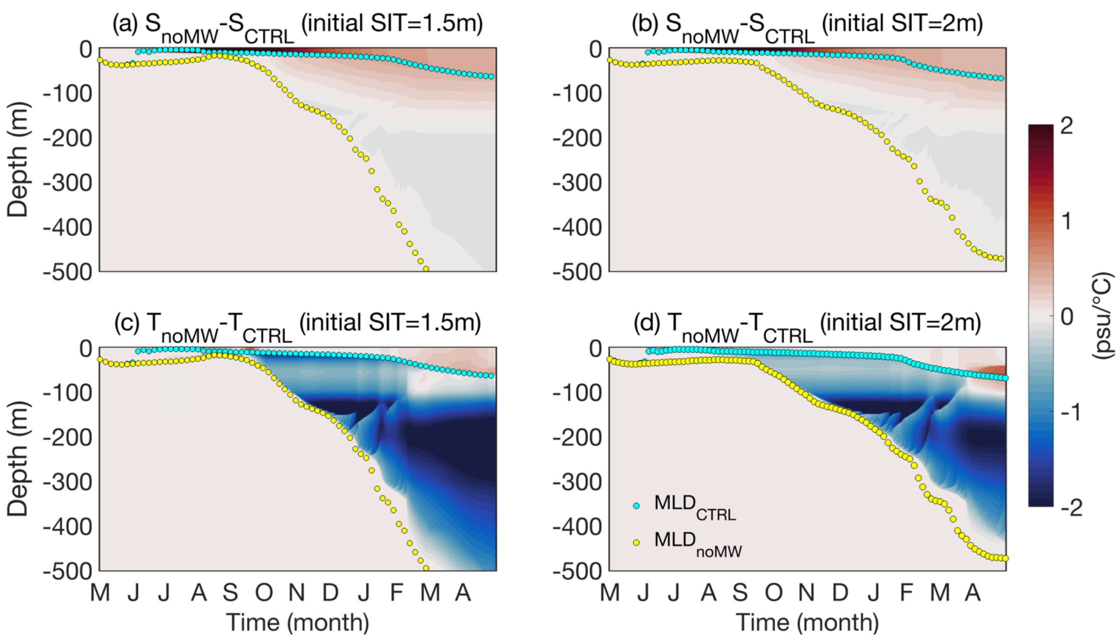

Figure S12. Modeled time series of ocean (a)-(b) salinity and (c)-(d) temperature differences in the WNS (noMW mins CTRL), using the WOA climatological data as the initial conditions. Left column: experiments with initial SIT of 1.5 m. Right column: experiments with initial SIT of 2 m. Colored dots indicate the MLD.

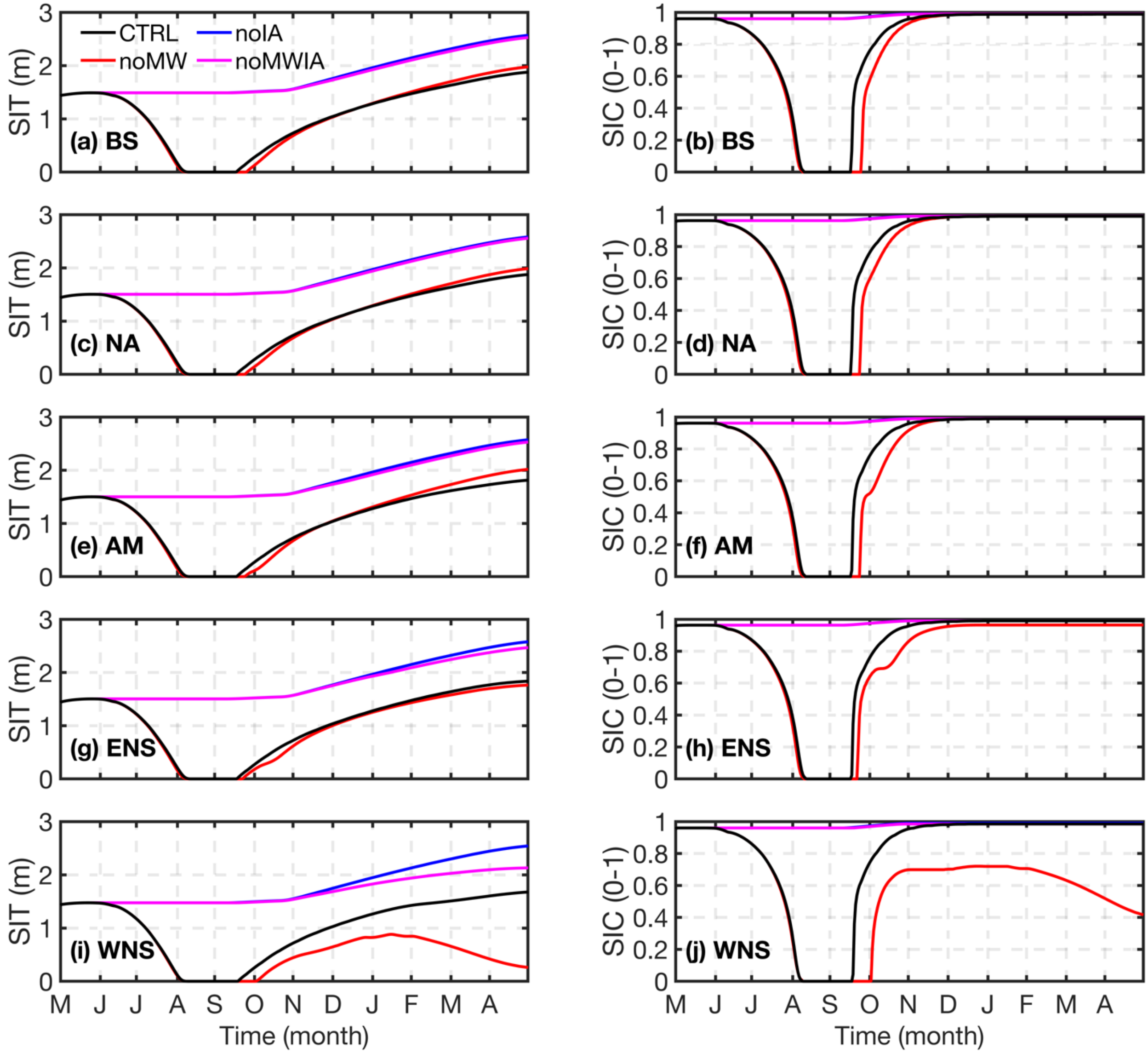

Figure S13. Modeled time development of SIT (left column) and SIC (right column) in all sub-regions, using WOA climatological data as the initial condition for experiments with initial SIT of 1.5 m.

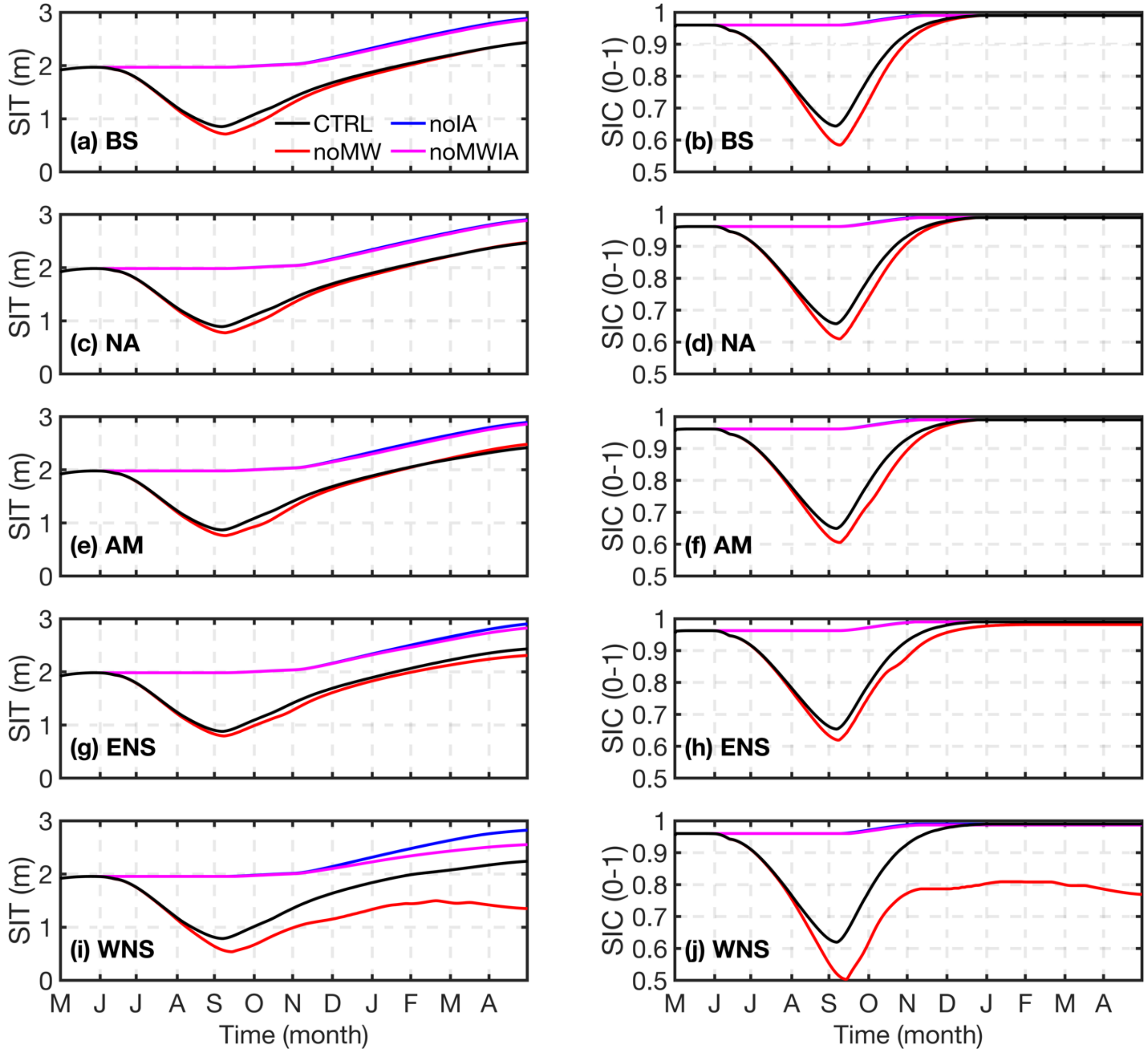

Figure S14. Same as Figure S17 but for the experiments with initial SIT of 2 m.

References

Bitz, C. M. and Lipscomb, W. H.: An energy-conserving thermodynamic model of sea ice, J. Geophys. Res., 104, 15669–15677, https://doi.org/10.1029/1999JC900100, 1999.

Haine, T. W. N., Curry, B., Gerdes, R., Hansen, E., Karcher, M., Lee, C., Rudels, B., Spreen, G., De Steur, L., Stewart, K. D., and Woodgate, R.: Arctic freshwater export: Status, mechanisms, and prospects, Global and Planetary Change, 125, 13–35, https://doi.org/10.1016/j.gloplacha.2014.11.013, 2015.

Jackson, J. M., Carmack, E. C., McLaughlin, F. A., Allen, S. E., and Ingram, R. G.: Identification, characterization, and change of the near-surface temperature maximum in the Canada Basin, 1993–2008, J. Geophys. Res., 115, 2009JC005265, https://doi.org/10.1029/2009JC005265, 2010.

Krishfield, R. A. and Perovich, D. K.: Spatial and temporal variability of oceanic heat flux to the Arctic ice pack, J. Geophys. Res., 110, 2004JC002293, https://doi.org/10.1029/2004JC002293, 2005.

Landy, J. C., Dawson, G. J., Tsamados, M., Bushuk, M., Stroeve, J. C., Howell, S. E. L., Krumpen, T., Babb, D. G., Komarov, A. S., Heorton, H. D. B. S., Belter, H. J., and Aksenov, Y.: A year-round satellite sea-ice thickness record from CryoSat-2, Nature, 609, 517–522, https://doi.org/10.1038/s41586-022-05058-5, 2022.

Large, W. G., McWilliams, J. C., and Doney, S. C.: Oceanic vertical mixing: A review and a model with a nonlocal boundary layer parameterization, Reviews of Geophysics, 32, 363–403, https://doi.org/10.1029/94RG01872, 1994.

Light, B., Smith, M. M., Perovich, D. K., Webster, M. A., Holland, M. M., Linhardt, F., Raphael, I. A., Clemens-Sewall, D., Macfarlane, A. R., Anhaus, P., and Bailey, D. A.: Arctic sea ice albedo: Spectral composition, spatial heterogeneity, and temporal evolution observed during the MOSAiC drift, Elementa: Science of the Anthropocene, 10, 000103, https://doi.org/10.1525/elementa.2021.000103, 2022.

Maykut, G. A. and McPhee, M. G.: Solar heating of the Arctic mixed layer, Journal of Geophysical Research: Oceans, 100, 24691–24703, https://doi.org/10.1029/95JC02554, 1995.

McPhee, M. G., Kikuchi, T., Morison, J. H., and Stanton, T. P.: Ocean-to-ice heat flux at the North Pole environmental observatory, Geophysical Research Letters, 30, 2003GL018580, https://doi.org/10.1029/2003GL018580, 2003.

Paulson, C. A., and J. J. Simpson: Irradiance Measurements in the Upper Ocean. J. Phys. Oceanogr., 7, 952–956, https://doi.org/10.1175/1520-0485(1977)007<0952:IMITUO>2.0.CO;2, 1977

Peralta-Ferriz, C. and Woodgate, R. A.: Seasonal and interannual variability of pan-Arctic surface mixed layer properties from 1979 to 2012 from hydrographic data, and the dominance of stratification for multiyear mixed layer depth shoaling, Progress in Oceanography, 134, 19–53, https://doi.org/10.1016/j.pocean.2014.12.005, 2015.

Polyakov, I. V., Pnyushkov, A. V., Alkire, M. B., Ashik, I. M., Baumann, T. M., Carmack, E. C., Goszczko, I., Guthrie, J., Ivanov, V. V., Kanzow, T., Krishfield, R., Kwok, R., Sundfjord, A., Morison, J., Rember, R., and Yulin, A.: Greater role for Atlantic inflows on sea-ice loss in the Eurasian Basin of the Arctic Ocean, Science, 356, 285–291, https://doi.org/10.1126/science.aai8204, 2017.

Steele, M., Ermold, W., and Zhang, J.: Modeling the formation and fate of the near-surface temperature maximum in the Canadian Basin of the Arctic Ocean, J. Geophys. Res., 116, 2010JC006803, https://doi.org/10.1029/2010JC006803, 2011.

Winton, M.: A Reformulated Three-Layer Sea Ice Model, J. Atmos. Oceanic Technol., 17, 525–531, https://doi.org/10.1175/1520-0426(2000)017%253C0525:ARTLSI%253E2.0.CO;2, 2000.

Zhong, W., Cole, S. T., Zhang, J., Lei, R., and Steele, M.: Increasing Winter Ocean-to-Ice Heat Flux in the Beaufort Gyre Region, Arctic Ocean Over 2006–2018, Geophysical Research Letters, 49, e2021GL096216, https://doi.org/10.1029/2021GL096216, 2022.